Electrostatic energy and phonon properties of Yukawa crystals

A. Kozhberov*
Ioffe Institute, Politekhnicheskaya 26, Saint Petersburg 194021, Russia

(Received 18 June 2018; published 14 December 2018)

We study electrostatic and phonon properties of Yukawa crystals. It is shown that in the harmonic approximation these systems which are used in the theory of dusty plasma can be described analytically by the model from the theory of neutron stars and white dwarfs. Using this approximation, we consider properties of body-centered-cubic (bcc), face-centered-cubic (fcc), hexagonal-close-packed (hcp), and MgB_2 lattices. Studies of MgB_2 and hcp lattices in the context of Yukawa systems are lacking. It is shown that they never possess the smallest potential energy and the phase diagram of stable Yukawa crystals contains bcc and fcc lattices only. However, corrections to the charge density proportional to $(\kappa a)^4$ can noticeably change the structural diagram of Yukawa systems. The analytical model developed also allows us to describe low-temperature effects where numerical simulations are difficult.

DOI: 10.1103/PhysRevE.98.063205

I. INTRODUCTION

A Yukawa system is a system of pointlike charged particles immersed in a neutralizing background. Usually it is assumed that all these particles are identical and have the electric charge $-Ze$ and mass M, where e is the electron charge absolute value. The background in the Yukawa systems is nonuniform and can be described by the inverse screening length κ. For instance, if the background consists of electrons, $\kappa \equiv \sqrt{4\pi e^2 \partial n_e/\partial \mu_e}$, where n_e and μ_e are electron mean number density and chemical potential, respectively. Systems with a uniform background are called Coulomb systems. These systems are widely used in various branches of physics.

It is believed that the matter in degenerate stars, namely, in white dwarf cores and neutron star crusts at not too low densities, consists of atomic nuclei (ions) immersed in a neutralizing background of electrons [1]. As a star cools, ions crystallize (see, e.g., [2,3]). According to Ref. [4], this crystallization process has been inferred from observations of oscillations of a white dwarf, while observations of transients indicate that the neutron star crust is solid [5–7]. In degenerate stars electrons are mostly strongly degenerate and can be characterized by the Thomas-Fermi wave vector $\kappa_{\rm TF} \approx 0.185 Z^{1/3}(1+x_r^2)^{1/4}/x_r^{1/2}$, where $x_r \equiv p_F/m_e c$ is the electron relativity parameter, p_F is the electron Fermi momentum, and m_e is the electron mass (see, e.g., [8]). Notice that the ordered structures can form in red giants and brown dwarfs [9].

Yukawa systems are also widely used in dusty plasma physics (see, e.g., [10]). In the simplest model the dusty plasmas consist of charged dust grains and the background which is formed by nondegenerate ions and electrons (here we follow the model which was developed in [11,12]). For nondegenerate electrons $\partial n_e/\partial \mu_e = n_e/k_B T$ and similarly for ions. Hence, in this situation κ is the inverse Debye D length $\kappa_D^2 = \kappa_{De}^2 + \kappa_{Di}^2 \equiv 4\pi e^2 n_e/k_B T + 4\pi e^2 Z_i^2 n_i/k_B T$, where Z_i and n_i are the charge number and mean number density of background ions, respectively, T is the temperature of the system (the temperature of background ions is taken to be equal to the temperature of dust particles), and k_B is the Boltzmann constant.

Both such different systems can be described by a simple model called a Yukawa crystal, in which pointlike charged particles are arranged into a lattice and neutralizing background characterized by the parameter κ. In this paper we show that the results of molecular-dynamics simulations of Yukawa crystals [13,14] can be verified by the theoretical model which was developed in [8] for the degenerate stars (in [8] they are called Coulomb crystals with polarizable background).

Only the body-centered-cubic (bcc) and face-centered-cubic (fcc) lattices were considered in [8,14], as well as in some other theoretical parers (e.g., [15–18]) which, using different approaches, qualitatively and/or quantitatively prove the results of simulations from [14]. The three-dimensional (3D) hexagonal Yukawa crystals were studied by molecular-dynamics simulations in [14] for the bcc and fcc lattices. In contrast, it is known that the ground state of 2D crystals has hexagonal symmetry (see, e.g., [19]). Also laboratory experiments (in many experiments dusty plasmas are not a bulk 3D system because of the presence of different forces such as gravity, shadow forces, thermal forces, and some others and cannot be described by the model of the Yukawa crystal) show that the strongly coupled dusty plasma forms a complicated crystal structure (see, e.g., [10,20–25]). Analysis of experiments carried out on board the International Space Station under microgravity conditions shows that plasma crystals have a structure which contains numerous bcc, fcc, and hexagonal-close-packed (hcp) clusters with the prevailing contribution of the latter two [26,27]. Similar results give different computer simulations (see, e.g., [28–30]). Hence the formation of the hexagonal Yukawa crystals is quite probable.

*kozhberov@gmail.com

Despite the interest in the dusty systems, the structural diagram of Yukawa crystals has received relatively little attention. The transition between the bcc and fcc lattices was obtained from molecular-dynamics simulations in Ref. [31], developed in Ref. [14], and later was proved in a few papers (see, e.g., [16]). Transitions between other lattices have not been considered and the structural diagram has not been studied analytically. In the present work we study the properties of the hcp Yukawa crystal. In the harmonic lattice approximation we calculate its total potential energy as a sum of electrostatic energy, the energy of zero-point vibration, and phonon free energy. This total potential energy is used to study the structural transitions between the hcp and cubic (bcc and fcc) lattices in dusty plasmas. One of the advantages of the harmonic lattice approximation is the ability to take into account the low-temperature effects where numerical simulations are difficult to provide. The importance of high-order corrections to the charge density is also discussed.

II. ELECTROSTATIC ENERGY

Yukawa crystals were investigated in [12] via molecular-dynamics simulations in a cubical domain with the side length L and periodic boundary conditions. Its volume is $V \equiv L^3$ and N is the number of charged pointlike particles in the crystal. The total potential energy U of such systems is given by [Eq. (29) from [12]]

$$U = N\frac{Z^2e^2}{2}\left[\sum_{j'\neq j}\Phi(\mathbf{r}_j-\mathbf{r}_{j'}) - \frac{4\pi n}{\kappa_D^2} - \kappa_D + \sum_{m\neq 0}\frac{e^{-\kappa_D mL}}{mL}\right], \tag{1}$$

where

$$\Phi(\mathbf{r}) = \sum_{m\neq 0}\frac{\exp(-\kappa_D|\mathbf{r}-\mathbf{m}L|)}{|\mathbf{r}-\mathbf{m}L|}, \tag{2}$$

$\mathbf{m} = (m_1, m_2, m_3)$ denotes an integer triplet, and $n \equiv N/V$ is the mean number density of charged pointlike particles. According to the electroneutrality condition, $Zn = Z_i n_i - n_e$. The position of the jth particle in the crystal is given by the radius vector $\mathbf{r}_j = \mathbf{X}_j + \mathbf{u}_j$, where $\mathbf{X}_j$ is the particle equilibrium position and $\mathbf{u}_j$ is the displacement. Equation (1) was obtained from the Poisson equation

$$\Delta\Psi(\mathbf{r}) = -4\pi\rho(\mathbf{r}), \tag{3}$$

where the charge density

$$\rho(\mathbf{r}) = -Z\sum_j \delta(\mathbf{r}-\mathbf{r}_j) + Zn - \frac{\kappa_D^2}{4\pi}[\Psi(\mathbf{r}) - \overline{\Psi}], \tag{4}$$

where

$$\overline{\Psi} \equiv \frac{1}{V}\int_V \Psi(\mathbf{r})d\mathbf{r}. \tag{5}$$

In this approach, the variation of the potential $\Psi(\mathbf{r})$ over V should be much smaller than the thermal energy. The next-order correction to the charge density is proportional κ_D^4.

If all particles are fixed in their equilibrium positions, U reduces to the electrostatic (Madelung) energy U_M. For a lattice with $N_{\rm cell}$ particles in the elementary cell, equilibrium positions are given by $\mathbf{X}_j = \mathbf{X}_{lp} = \mathbf{R}_l + \boldsymbol{\chi}_p$, where $\mathbf{R}_l$ is the lattice vector, $\boldsymbol{\chi}_p$ is the basis vector of the p particle ($p = 1, \ldots, N_{\rm cell}$) in the elementary cell, and $l = (l_1, l_2, l_3)$ is the integer triplet. The reciprocal lattice is formed by vectors $\mathbf{G}_b$, where $\mathbf{b} = (b_1, b_2, b_3)$ is the integer triplet.

The Madelung energy U_M can be found analytically at fixed n and $L \to \infty$. Using the Ewald transformation, it is possible to derive a rapidly converging expression for the Madelung energy of the Yukawa lattice [8]

$$\begin{aligned}\frac{U_M}{NZ^2e^2} \equiv \frac{\zeta}{a} = {} & \frac{1}{N_{\rm cell}}\sum_{l,p,p'}(1-\delta_{l0}\delta_{pp'})\frac{E_- + E_+}{4Y_l} \\ & + \frac{1}{N_{\rm cell}^2}\sum_{b,p,p'}\frac{2\pi n}{G_b^2+\kappa^2}e^{-(G_b^2+\kappa^2)/4A^2}e^{-i\mathbf{G}_b(\boldsymbol{\chi}_p-\boldsymbol{\chi}_{p'})} \\ & - \frac{\kappa}{2}\mathrm{erf}\left(\frac{\kappa^2}{2A}\right) - \frac{A}{\sqrt{\pi}}e^{-\kappa^2/4A^2} - \frac{2\pi n}{\kappa^2},\end{aligned} \tag{6}$$

where $E_\pm = e^{\pm\kappa Y_l}[1 - \mathrm{erf}(AY_l \pm \kappa/2A)]$, $\mathrm{erf}(z)$ is the error function, $\mathbf{Y}_l = \mathbf{R}_l + \boldsymbol{\chi}_p - \boldsymbol{\chi}_{p'}$, and $a \equiv (4\pi n/3)^{-1/3}$ is the Wigner-Seitz radius. The parameter A is chosen in such a way that the summation over direct and reciprocal lattice vectors converges equally rapidly. For lattices in consideration, $Aa \approx 2$. The parameter ζ is called the Madelung constant. It depends on the type of lattice and κa. Equation (6) for U_M has the same form for κ_D and $\kappa_{\rm TF}$. For this reason the subscript in κ is omitted.

For lattices with $N_{\rm cell} = 1$ Eq. (6) was derived in [8] and was used for the bcc and fcc lattices. For lattices with $N_{\rm cell} > 1$, the expression for U_M is given here. In [13] the electrostatic energy was calculated from the molecular-dynamics simulations as a limiting value of U at $T \to 0$. Madelung constants for the bcc lattice obtained in [13] are given in Table I as $\zeta_{\rm HF}$. Our results based on Eq. (6) are given as ζ in Table I. For the bcc lattice they coincide with the results of [13,31], but more significant digits are given. For the fcc lattice both calculations are also consistent. Equation (6) allows us to calculate the Madelung energy for any lattice much more accurately and faster than molecular-dynamics simulations.

Usually (see, e.g., [32]), for the hcp lattice the distance between hexagonal layers h in the elementary cell is assumed to be $h_0 \equiv \sqrt{8/3}a_{\rm lat} \approx 1.632\,993 a_{\rm lat}$, where $a_{\rm lat}$ is the lattice constant. This value comes from the problem of close packing of equal spheres. However, in Yukawa crystals charged particles are pointlike and it is not obvious that the electrostatic energy of the hcp lattice achieves a minimum at $h = h_0$ in this case. It is more correct to consider the hcp lattice with $h = h_{\rm min}$ that corresponds to the minimum of U_M. The $h_{\rm min}$ values obtained for several κa are also presented in Table I. At $\kappa a = 0$ (uniform background) the Madelung energy of the hcp lattice reaches a minimum at $h_{\rm min} \approx 1.635\,639 a_{\rm lat} > h_0$. A similar situation is found at $0 < \kappa a < 5$: $h_{\rm min}/a_{\rm lat}$ is always slightly greater than $\sqrt{8/3}$ and decreases when κa increases. This small difference does not lead to a significant change of U_M. In Table I, $\zeta_{\rm min}$ corresponds to the minimum of the Madelung energy while ζ corresponds to the energy

TABLE I. Madelung constants of the bcc, fcc, hcp, and MgB_2 lattices.

	bcc lattice		fcc lattice		hcp lattice			MgB_2 lattice	
κa	$-\zeta_{HF}$	$-\zeta$	$-\zeta_{HF}$	$-\zeta$	h_{min}/a_{lat}	$-\zeta_{min}$	$-\zeta$	h_{min}/a_{lat}	$-\zeta$
0.0	0.895929	0.895929256	0.895873	0.895873616	1.635639	0.895838451	0.895838120	0.593936	0.894505630
0.2	0.900074	0.900073612	0.900020	0.900020482	1.635630	0.899985873	0.899985549	0.593958	0.898663839
0.5	0.921671	0.921671339	0.921631	0.921630646	1.635543	0.921598798	0.921598509	0.594074	0.920331769
1.0	0.996706	0.996706468	0.996701	0.996701309	1.635278	0.996677534	0.996677339	0.594458	0.995586492
2.0	1.269026	1.269025941	1.269079	1.269079142	1.634495	1.269071279	1.269071235	0.595636	1.268452721
3.0	1.651144	1.651143676	1.651194	1.651193657	1.633786	1.651192170	1.651192165	0.596801	1.650930425
4.0	2.091283	2.091283389	2.091309	2.091308661	1.633349	2.091308471	2.091308471	0.597578	2.091219086

at $h = h_0$. Previously such investigations were performed by Nagai and Fukuyama in [33] but for the Coulomb crystal only ($\kappa a = 0$). They obtained $h_{min} = 1.633 a_{lat}$ and suggested that $h_{min} = \sqrt{8/3} a_{lat}$.

In addition to the hcp lattice, we considered another lattice with hexagonal symmetry. We call it the MgB_2 lattice because it is the lattice of magnesium diboride under terrestrial conditions (space group $P6/mmm$). The MgB_2 lattice is a sequence of layers of magnesium and boron. The distance between adjacent layers is $h/2$, while a_{lat} is the distance between the nearest magnesium ions in the layer. The number of ions in the elementary cell is $N_{cell} = 3$. Here we consider only the one-component Yukawa MgB_2 lattice formed by identical charged particles. The parameter h is not fixed and is determined by the minimum of the Madelung energy. There is no experimental evidence that the MgB_2 lattice forms in Yukawa systems. However, this lattice possesses the fourth smallest Madelung constant after the bcc, fcc, and hcp lattices (among those known in the literature [34,35]). At $\kappa a = 0$, the Madelung constant of the one-component MgB_2 lattice is equal to $-0.894\,505\,630\,008$. In the MgB_2 lattice h_{min} slightly depends on κa (see Table I). As in the hcp lattice, this dependence does not affect the computations noticeably and can be neglected. Further, we consider that $h = \sqrt{8/3} a_{lat}$ in the hcp lattice and $h \approx 0.593\,936 a_{lat}$ in the MgB_2 lattice. Notice that the hexagonal lattice is not discussed because it is not stable in the harmonic lattice approximation [35], while the possibility of formation of this lattice was indicated in [36].

Madelung constants of the hcp and MgB_2 lattices are always larger than the Madelung constant of the fcc lattice (see Table I). At $\kappa a < 1.065\,714$ the bcc lattice has the lowest U_M among all lattices in consideration, while at $\kappa a > 1.065\,714$ the fcc lattice has the lowest U_M. This result agrees with Ref. [13].

In [13] the electrostatic energy of the bcc Yukawa lattice was obtained by molecular-dynamics simulations and fitted for $\kappa a < 1$ by a polynomial [Eq. (15) from Ref. [13]]. Our investigations allow us to improve this approximation. An equation for the electrostatic energy at small κa can be obtained analytically from the expansion of Eq. (6). It is clear from Eq. (6) that this approximation should contain only even powers of κa, while the fit from Ref. [13] keeps all powers:

$$U_M^{bcc} = -N\frac{Z^2e^2}{a}[0.895\,929\,255\,7 + 0.103\,732\,333\,7(\kappa a)^2 - 0.003\,091\,327\,0(\kappa a)^4 + 0.000\,143\,040\,0(\kappa a)^6 - 7.1863\times10^{-6}(\kappa a)^8]. \quad (7)$$

This equation represents U_M with an accuracy of eight significant digits for $\kappa a < 0.5$. A similar equation can be written for the fcc, hcp, and MgB_2 lattices,

$$U_M = -N\frac{Z^2e^2}{a}[\zeta_0 + \zeta_2(\kappa a)^2 + \zeta_4(\kappa a)^4 + \zeta_6(\kappa a)^6 + \zeta_8(\kappa a)^8], \quad (8)$$

where the parameters ζ_i are given in Table II.

Equation (1) gives the correct expression for the terms in the potential energy proportional to $(\kappa a)^0$ and $(\kappa a)^2$. Corrections to the charge density of the order of $(\kappa a)^4$ make the same order changes to the potential energy. At the same time, the differences between the energies are extremely small and corrections of the order of $(\kappa a)^4$ and higher can radically change the structural diagram of the Yukawa crystals. The importance of these corrections is easy to illustrate by a comparison of the first two terms in Eq. (8). Let us define the reduced electrostatic energy as

$$U_{M2} \equiv -N\frac{Z^2e^2}{a}[\zeta_0 + \zeta_2(\kappa a)^2]. \quad (9)$$

Retention of only the first two terms in U_M leads to transformations of structural transitions. Indeed, at low κa the lowest U_{M2} has the bcc lattice, at $0.937\,15 < \kappa a < 1.583\,01$ the fcc

TABLE II. Parameters ζ_i for the Madelung energy of the fcc, hcp, and MgB_2 lattices.

ζ_i	fcc	hcp	MgB_2
ζ_0	0.8958736152	0.8958381205	0.8945056294
ζ_2	0.1037956875	0.1040806163	0.1038098518
ζ_4	-0.0031060725	-0.0031410914	-0.0031091345
ζ_6	0.0001451182	0.0001485484	0.0001455958
ζ_8	-7.4104×10^{-6}	-7.4708×10^{-6}	-7.7141×10^{-6}

lattice, at $1.583\,01 < \kappa a < 2.218\,38$ the hcp lattice, and at $\kappa a > 2.218\,38$ the MgB_2 lattice.

III. ZERO-POINT ENERGY

Pointlike charged particles in the crystal are not fixed and actually oscillate around their equilibrium positions even at $T = 0$ due to the quantum zero-point vibrations. The frequencies of these oscillations, ω_ν, can be found from the dispersion equation

$$\det\left\{D^{\alpha\beta}_{pp'}(\mathbf{k}) - \omega^2_\nu(\mathbf{k})\delta^{\alpha\beta}\delta_{pp'}\right\} = 0, \tag{10}$$

where the indices α and β denote Cartesian components, p and p' run over the charged pointlike particles in the elementary cell, ν enumerates the oscillation modes ($\nu = 1, \ldots, 3N_{\rm cell}$) at a given wave vector $\mathbf{k}$, and $D^{\alpha\beta}_{pp'}(\mathbf{k})$ is the dynamic matrix. The dynamic matrix of the Yukawa crystal with $N_{\rm cell} = 1$ was derived in [8]. An equation for the dynamic matrix with arbitrary $N_{\rm cell}$ is given by Eq. (A1) from [37], where the phonon properties were discussed in detail. It is instructive to compare the phonon spectrum obtained in [37] with the results of molecular-dynamics simulations directly and it will be done separately. Here we consider only the average over the volume phonon properties.

The dispersion Eq. (10) allows to calculate the phonon spectrum at any wave vector $\mathbf{k}$. Due to the periodicity of the crystal lattice, it is sufficient to calculate $\omega_\nu(\mathbf{k})$ only in the first Brillouin zone. Let us define the average of any function $f(\omega)$ of phonon frequencies over the volume of the first Brillouin zone $V_{\rm BZ} = (2\pi)^3 n/N_{\rm cell}$,

$$\langle f(\omega)\rangle = \frac{1}{3N_{\rm cell}}\sum_{\nu=1}^{3N_{\rm cell}}\frac{1}{V_{\rm BZ}}\int_{\rm BZ} f(\omega_\nu(\mathbf{k}))d\mathbf{k}. \tag{11}$$

Then the zero-point energy of the crystal is

$$E_0 \equiv 1.5N\hbar\langle\omega\rangle = 1.5N\hbar\omega_p u_1, \tag{12}$$

where $u_1 = \langle\omega/\omega_p\rangle$ is the first frequency moment, $\omega_p = \sqrt{4\pi n Z^2 e^2/M}$ is the plasma frequency, and $\hbar$ is the Plank constant.

In the Yukawa crystal, u_1 depends on the lattice type and κa. In [8] the first moments of the bcc and fcc lattices were investigated and approximated for $\kappa a \ll 1$. The u_1 value of the hcp lattice is considered here. The one-component MgB_2 lattice is found to be unstable. At some $\mathbf{k}$, modes with $\omega^2_\nu(\mathbf{k}) < 0$ appear in its phonon spectrum. Therefore, the phonon properties of the one-component MgB_2 lattice are not considered. It is interesting to note that at $\kappa a = 0$ the MgB_2 lattice with two different ions in the elementary cell (their charges are Z_1 and $Z_2 \neq Z_1$) is stable at some values of h and Z_2/Z_1. The bcc lattice is unstable at $\kappa a > 4.76$, in accordance with previous studies [31]. The fcc and hcp lattices are stable until $\kappa a = 5$ and we do not study these lattices at higher κa.

The ratios $u_1^{\rm fcc}/u_1^{\rm bcc} - 1$, $u_1^{\rm hcp}/u_1^{\rm bcc} - 1$, and $u_1^{\rm hcp}/u_1^{\rm fcc} - 1$ are plotted in Fig. 1. At $\kappa a = 0$, $u_1^{\rm bcc} = 0.511\,387\,7$, $u_1^{\rm fcc} = 0.513\,194$, and $u_1^{\rm hcp} = 0.513\,336\,9$. The relation $u_1^{\rm hcp} > u_1^{\rm fcc} > u_1^{\rm bcc}$ holds for any value of $\kappa a \geqslant 0$. In other words, the bcc lattice possesses the smallest zero-point energy at any κa. At $T = 0$, the total energy of the Yukawa crystal is

$$U_0 \equiv U_M + E_0 = NT_p(\Gamma_p\zeta + 1.5u_1), \tag{13}$$

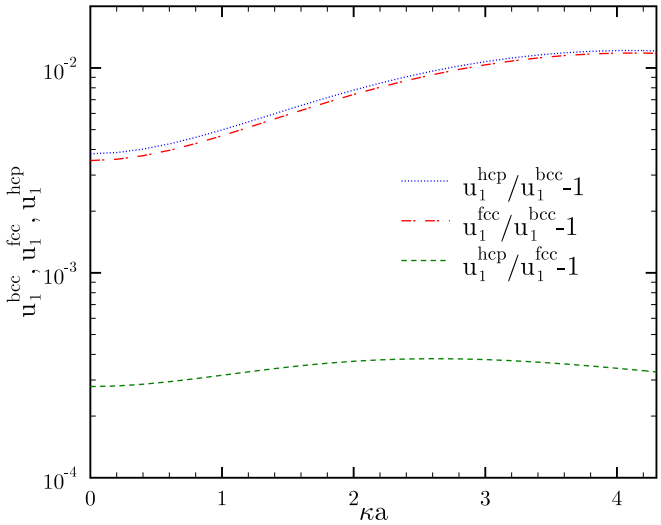

FIG. 1. Ratios of lattice moments u_1 of the bcc, fcc, and hcp lattices.

where $T_p = \hbar\omega_p$ is the plasma temperature. At $T = 0$, the total energy is a function of two parameters, κa and $\Gamma_p \equiv Z^2e^2/a\hbar\omega_p$. In Fig. 2 we plot the dependence of Γ_p on κa for which the total energy of the bcc lattice ($U_0^{\rm bcc}$) is equal to the total energy of the fcc lattice ($U_0^{\rm fcc}$). Above this curve, the energy of the fcc lattice is smaller than the energy of the fcc lattice. At $\Gamma_p \to \infty$ the energy of the zero-point vibrations can be neglected and κa tends to 1.066.

The dynamic matrix of the Yukawa crystals was derived from the same equation for the potential energy as the electrostatic energy, therefore U_M and E_0 have similar precision. At the same time, $|u_1^{\rm fcc} - u_1^{\rm bcc}| \gg |\zeta^{\rm fcc} - \zeta^{\rm bcc}|$. Hence corrections to the zero-point energy proportional to $(\kappa a)^4$ do not influence significantly the transitions between lattices.

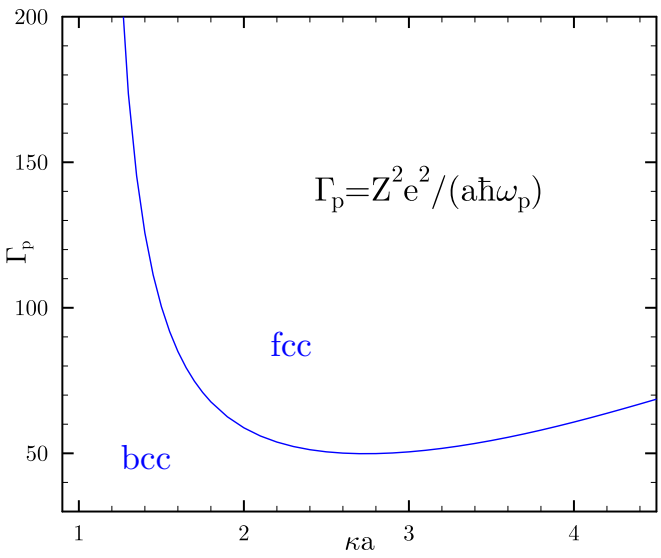

FIG. 2. Dependence of Γ_p on κa under the condition $U_0^{\rm bcc} = U_0^{\rm fcc}$. The curve shows the structural transition between the bcc and fcc Yukawa lattices at $T = 0$ if the electrostatic and zero-point energies are taken into account.

IV. THERMAL CONTRIBUTION TO THE POTENTIAL ENERGY

The phonon thermal contribution $F_{\rm th}$ to the total potential energy (thermal free energy) is equal to

$$F_{\rm th} = 3NT\langle \ln(1-e^{-w})\rangle, \tag{14}$$

where $w \equiv \hbar\omega_\nu(\mathbf{k})/T$ (see, e.g., [32]). For the bcc Yukawa lattice it was considered in [8]. Here we extend this study to other lattice types. In Fig. 3 we plot the ratios $F_{\rm th}^{\rm fcc}/F_{\rm th}^{\rm bcc}$ and $F_{\rm th}^{\rm hcp}/F_{\rm th}^{\rm bcc}$ as functions of $t \equiv T/T_p$ for various values of κa. These ratios were discussed in [38] for crystals with a uniform background ($\kappa a = 0$). At $\kappa a = 1$ and $\kappa a = 0.5$ they have the same features as at $\kappa a = 0$. For instance, at high and medium temperatures ($T \gtrsim 10^{-2}T_p$) and any κa, $F_{\rm th}^{\rm hcp}$ and $F_{\rm th}^{\rm fcc}$ are greater than $F_{\rm th}^{\rm bcc}$ ($F_{\rm th}$ is negative). At $\kappa a = 1$, the ratio $F_{\rm th}^{\rm hcp}/F_{\rm th}^{\rm bcc}$ reaches a minimum of approximately 0.7425 at $t \approx 0.034\,83$, while a minimum of $F_{\rm th}^{\rm fcc}/F_{\rm th}^{\rm bcc}$ is approximately 0.8072 at $t \approx 0.039\,26$. In the quantum limit, $F_{\rm th}^{\rm hcp} < F_{\rm th}^{\rm fcc} < F_{\rm th}^{\rm bcc}$ for any κa. At $T \ll T_p$, the ratios $F_{\rm th}^{\rm hcp}/F_{\rm th}^{\rm bcc}$ and $F_{\rm th}^{\rm hcp}/F_{\rm th}^{\rm fcc}$ decrease with an increase of κa. At $\kappa a = 1$ they reach 1.066 and 1.0104, respectively. Figure 3 shows that phonon thermodynamic properties of different lattices at fixed κa and t may vary from each other by tens of percent.

V. TOTAL POTENTIAL ENERGY

In the harmonic approximation the total potential energy U (which would more accurately be called free energy but we use the same notation as in [14]) at any T consists of three parts: the electrostatic (Madelung) energy U_M, the zero-point energy E_0, and the thermal contribution $F_{\rm th}$. At $T \lesssim 5\times 10^{-3}T_p$, the thermal contribution does not play a noticeable role and can be neglected. At these low temperatures it is enough to use Eq. (13).

At high temperatures ($T \gg T_p$)

$$F_{\rm th} \approx 3NT[u_{\rm ln} - \ln t] - 1.5N\omega_p u_1, \tag{15}$$

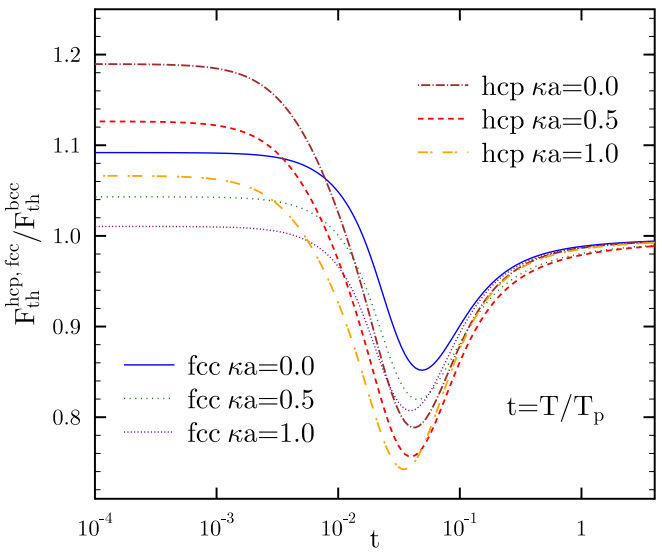

FIG. 3. Ratios of $F_{\rm th}$ of the bcc, fcc, and hcp lattices.

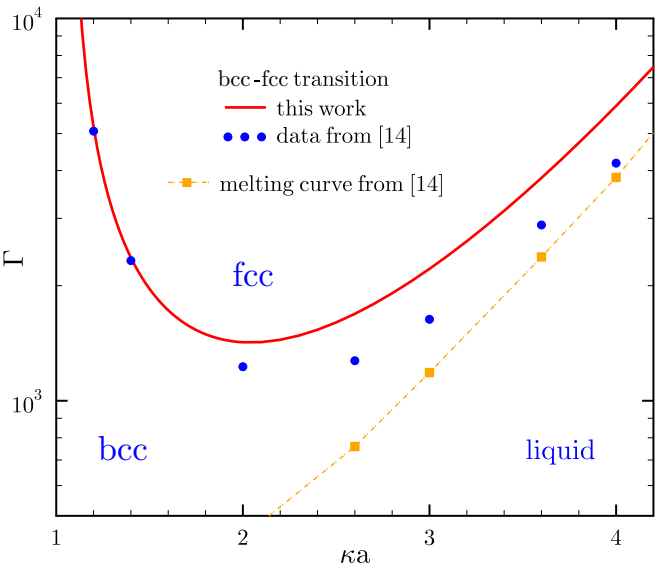

FIG. 4. Phase diagram of Yukawa systems at $T \gg T_p$. Squares and circles are the results of molecular-dynamics simulations from [14] and the solid line is the result of the harmonic lattice approximation.

where $u_{\rm ln} = \langle \ln(\omega/\omega_p)\rangle$. At $\kappa a = 0$, $u_{\rm ln}^{\rm bcc} = -0.831\,295$, which is less than $u_{\rm ln}^{\rm fcc} = -0.817\,908\,5$ and $u_{\rm ln}^{\rm hcp} = -0.816\,031$. This situation holds at $\kappa a > 0$. For instance, at $\kappa a = 1$, $u_{\rm ln}^{\rm bcc} = -0.994\,814$, $u_{\rm ln}^{\rm fcc} = -0.978\,198$, and $u_{\rm ln}^{\rm hcp} = -0.976\,292$. At any κa, the bcc lattice possesses the smallest $u_{\rm ln}$. The total potential energy U is

$$\frac{U}{NT} = \Gamma\zeta + \frac{1.5u_1}{t} + \frac{F_{\rm th}}{NT} = \Gamma\zeta + 3[u_{\rm ln} - \ln t], \tag{16}$$

where $\Gamma \equiv Z^2e^2/aT = \Gamma_p/t$ is the Coulomb coupling parameter. Hence, at high temperatures, the difference between the total potential energy of different lattices is independent of t and can be considered as a function of Γ and κa only.

The structural transition curve between the bcc and fcc lattices at $T \gg T_p$ is plotted in Fig. 4. The solid line shows the result of our analytical calculations. It is similar to Fig. 2, but now the high-temperature limit is used. In the harmonic approximation $U^{\rm bcc} = U^{\rm fcc}$ at

$$\Gamma_b = 3\frac{u_{\rm ln}^{\rm fcc} - u_{\rm ln}^{\rm bcc}}{\zeta^{\rm bcc} - \zeta^{\rm fcc}}. \tag{17}$$

The parameter Γ_b is given in Table III for several κa. Values of Γ_b obtained from the molecular-dynamics simulations in

TABLE III. Values of $\Gamma_b^{\rm FHD}$ and Γ_b for some κa.

κa	$\Gamma_b^{\rm FHD}$	Γ_b	$\Gamma_b^{\rm an}$
1.2	5070	5201	5094
1.4	2325	2369	2334
2.0	1228	1422	1232
2.6	1273	1688	1274
3.6	2884	3827	2882

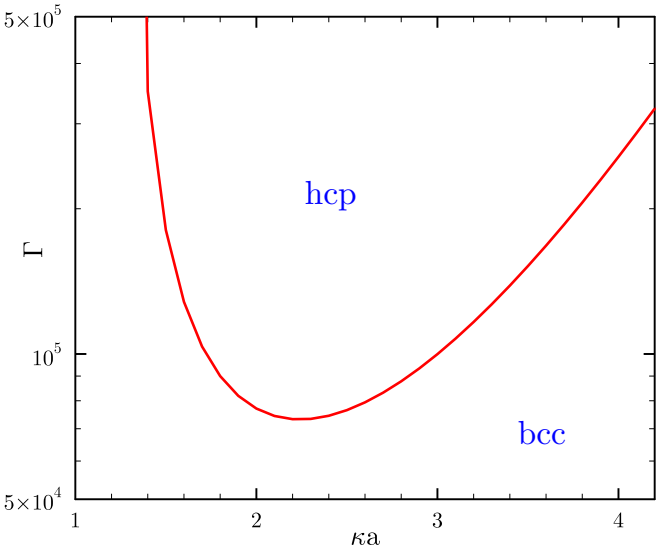

FIG. 5. Structural transition curve between the bcc and hcp Yukawa lattices at $T \gg T_p$ in the harmonic lattice approximation.

[14] are shown with points in Fig. 4 and given in the $\Gamma_b^{\rm FHD}$ column in Table III. At $\kappa a < 2$ and far from the melting curve (dash-dotted line in Fig. 4), the difference between Γ_b and $\Gamma_b^{\rm FHD}$ is small. At higher κa the discrepancy between our results and those of [14] can be explained by the absence of anharmonic corrections in our calculations. Analytically, the first-order anharmonic correction to the energy of the Coulomb crystal was calculated in Ref. [39]; for crystals with $\kappa a > 0$ no comparison is available. In Ref. [14] the correction was approximated from numerical results as $A_1/\Gamma + A_2/\Gamma^2$. Notice that $|A_1| \ll |A_2|$. If we add them to our calculations we obtain a different Γ_b. In Table III this Γ_b is denoted by $\Gamma_b^{\rm an}$ and it agrees better with $\Gamma_b^{\rm FHD}$. The remaining differences,

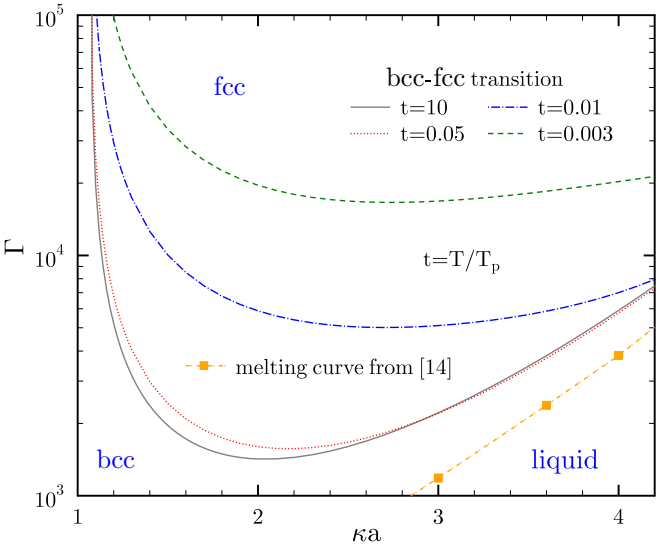

FIG. 6. Phase diagram of Yukawa systems at different $T \lesssim T_p$. Squares are the results of molecular-dynamics simulations from [14] and lines are the results of the harmonic lattice approximation.

especially at $\kappa a = 1.2$ and 1.4, can be explained by the insufficient accuracy of previous computations. Near $\kappa a = 1.066$, Γ_b grows very fast, so high-precision calculations are needed.

The total energy of the hcp lattice is always higher than the total energy of the fcc lattice, but a transition between the bcc and hcp lattices can occur. It is plotted in Fig. 5. Typical values of Γ_b for this transition are an order of magnitude higher that the typical values of Γ_b for the bcc-fcc transition and for the phase transition between solid and liquid. In addition, $U^{\rm bcc} < U^{\rm hcp}$ at any Γ if $\kappa a < 1.307\,20$.

In contrast to classical molecular-dynamics simulations, the harmonic approximation allows us to calculate the total energy of Yukawa crystals at $T \lesssim T_p$. At such T, precise calculations of $F_{\rm th}$ should be used. According to Eq. (14), the difference between the energies of the lattices is a function of κa, t, and Γ. In Fig. 6 we plot the dependence of Γ_b on κa for $t = 10$, 0.05, 0.01, and 0.003. The solid curve for $t = 10$ coincides with the solid curve in Fig. 4. A decrease of temperature leads to an increase in Γ_b. At low temperatures, the thermal contribution can be neglected and $\Gamma_b \propto 1/t$.

VI. CONCLUSION

The model of a crystal formed by pointlike ions in the polarized electron background is widely used in the theory of neutron stars and white dwarfs (see, e.g., [8]). It turns out that this model is similar to the model of a dusty strongly coupled Yukawa crystal (see, e.g., [12]). It is shown that the electrostatic energy in both models is described by the same analytical equation.

The electrostatic and thermodynamical properties of Yukawa crystals at $T \gg T_p$ were widely investigated in [11–14] by molecular-dynamics simulations. In this paper we used the harmonic lattice approximation to calculate the total potential energy of such crystals and to verify the results from Ref. [14] independently. In the harmonic approximation the total potential energy is the sum of electrostatic (Madelung), zero-point, and thermal free energies where the latter two contributions can be obtained from the phonon spectrum of the lattice. This approximation is successfully used to study the properties of crystals far from the melting point. Therefore, at $\kappa a < 2$ the structural transition between the bcc and fcc lattices, which was obtained from molecular-dynamics simulations in Ref. [14], is analytically proved by our model (at $T \gg T_p$ the structural transition between lattices depends on κa and Γ). At higher κa the structural transition between the bcc and fcc lattices takes place near the melting curve (transition between the bcc lattice and the Yukawa liquid), where the anharmonically correct ions need to be taken into account.

Analytical harmonic calculations allow us to consider other Yukawa lattices. In addition to the bcc and fcc lattices we considered the hcp and MgB_2 lattices. It was shown that the MgB_2 lattice is unstable. In contrast, the total potential energy of the hcp lattice is always greater than the total potential energy of the fcc lattice, so the structural transition studied herein does not appear. Note that the difference between the energies of the bcc and fcc lattices is too small and next-order

corrections to the charge density can in principle lead to the appearance the transition.

The harmonic model allows us to consider low-temperature effects which are difficult to examine by numerical simulations. At $T \lesssim T_p$ the total potential energy depends on κa, Γ, and t.

ACKNOWLEDGMENTS

The author is deeply grateful to P. S. Shternin for valuable comments on the paper. The work was partially supported by the Presidium of the Russian Academy of Sciences Program No. 13 "Condensed matter and plasmas at high energy densities."

[1] S. L. Shapiro and S. A. Teukolsky, *Black Holes, White Dwarfs, and Neutron Stars* (Wiley-Interscience, New York, 1983).

[2] C. J. Horowitz and D. K. Berry, Phys. Rev. C **79**, 065803 (2009).

[3] P. Haensel, A. Y. Potekhin, and D. G. Yakovlev, *Neutron Stars 1: Equation of State and Structure* (Springer, New York, 2007).

[4] D. E. Winget, S. O. Kepler, F. Campos, M. H. Montgomery, L. Girardi, P. Bergeron, and K. Williams, Astrophys. J. **693**, L6 (2009).

[5] E. M. Cackett, R. Wijnands, M. Linares, J. M. Miller, J. Homan, and W. H. G. Lewin, Mon. Not. R. Astron. Soc. **372**, 479 (2006).

[6] P. S. Shternin, D. G. Yakovlev, P. Haensel, and A. Y. Potekhin, Mon. Not. R. Astron. Soc. **382**, L43 (2007).

[7] E. F. Brown and A. Cumming, Astrophys. J. **698**, 1020 (2009).

[8] D. A. Baiko, Phys. Rev. E **66**, 056405 (2002).

[9] V. E. Fortov and G. E. Morfil, *Complex and Dusty Plasmas: From Laboratory to Space* (CRC, Portland, 2009).

[10] V. E. Fortov, A. V. Ivlev, S. A. Khrapak, A. G. Khrapak, and G. E. Morfill, Phys. Rep. **421**, 1 (2005).

[11] R. T. Farouki and S. Hamaguchi, Phys. Rev. E **47**, 4330 (1993).

[12] S. Hamaguchi and R. T. Farouki, J. Chem. Phys. **101**, 9876 (1994).

[13] R. T. Farouki and S. Hamaguchi, J. Chem. Phys. **101**, 9885 (1994).

[14] S. Hamaguchi, R. T. Farouki, and D. H. E. Dubin, Phys. Rev. E **56**, 4671 (1997).

[15] A.-P. Hynninen and M. Dijkstra, Phys. Rev. E **68**, 021407 (2003).

[16] R. S. Hoy and M. O. Robbins, Phys. Rev. E **69**, 056103 (2004).

[17] S. A. Khrapak and G. E. Morfill, Europhys. Lett. **100**, 66004 (2012).

[18] O. S. Vaulina and X. G. Koss, Phys. Rev. E **92**, 042155 (2015).

[19] M. Bonitz, P. Ludwig, H. Baumgartner, C. Henning, A. Filinov, D. Block, O. Arp, A. Piel, S. Kading, Y. Ivanov, A. Melzer, H. Fehske, and V. Filinov, Phys. Plasmas **15**, 055704 (2008).

[20] V. E. Fortov, A. G. Khrapak, S. A. Khrapak, V. I. Molotkov, and O. F. Petrov, Phys. Usp. **47**, 447 (2004).

[21] G. E. Morfill and H. Thomas, J. Vac. Sci. Technol. A **14**, 490 (1996).

[22] J. H. Chu and Lin I, Phys. Rev. Lett. **72**, 4009 (1994).

[23] H. Thomas, G. E. Morfill, V. Demmel, J. Goree, B. Feuerbacher, and D. Mohlmann, Phys. Rev. Lett. **73**, 652 (1994).

[24] T. Trottenberg, A. Melzer, and A. Piel, Plasma Sources Sci. Technol. **4**, 450 (1995).

[25] M. Zuzic, A. V. Ivlev, J. Goree, G. E. Morfill, H. M. Thomas, H. Rothermel, U. Konopka, R. Sutterlin, and D. D. Goldbeck, Phys. Rev. Lett. **85**, 4064 (2000).

[26] B. A. Klumov, Phys. Usp. **53**, 1053 (2010).

[27] B. Klumov, P. Huber, S. Vladimirov, H. Thomas, A. Ivlev, G. Morfill, V. Fortov, A. Lipaev, and V. Molotkov, Plasma Phys. Contr. Fusion **51**, 124028 (2009).

[28] C. Desgranges and J. Delhommelle, J. Chem. Phys. **126**, 054501 (2007).

[29] I. Rios de Anda, A. Statt, F. Turci, and C. P. Royall, Contrib. Plasma Phys. **55**, 172 (2015).

[30] M. Bonitz, D. Block, O. Arp, V. Golubnychiy, H. Baumgartner, P. Ludwig, A. Piel, and A. Filinov, Phys. Rev. Lett. **96**, 075001 (2006); M. Bonitz, C. Henning, and D. Block, Rep. Prog. Phys. **73**, 066501 (2010).

[31] M. O. Robbins, K. Kremer, and G. S. Grest, J. Chem. Phys. **88**, 3286 (1988).

[32] D. A. Baiko, A. Y. Potekhin, and D. G. Yakovlev, Phys. Rev. E **64**, 057402 (2001).

[33] T. Nagai and H. Fukuyama, J. Phys. Soc. Jpn. **52**, 44 (1983).

[34] N. Chamel and A. F. Fantina, Phys. Rev. C **94**, 065802 (2016).

[35] A. A. Kozhberov, Ph.D. thesis, Ioffe Institute, 2018.

[36] J. B. Pieper, J. Goree, and R. A. Quinn, Phys. Rev. E **54**, 5636 (1996).

[37] A. A. Kozhberov and D. A. Baiko, Phys. Plasmas **24**, 112704 (2017).

[38] A. A. Kozhberov and D. A. Baiko, Astrophys. Space Sci. **359**, 50 (2015).

[39] D. H. E. Dubin, Phys. Rev. A **42**, 4972 (1990).